Elongational Viscosity of Narrow Molar Mass Distribution Polystyrene

Anders Bach,[†] Kristoffer Almdal,[§] Henrik Koblitz Rasmussen,[‡] and Ole Hassager*[,†]

The Danish Polymer Centre, Department of Chemical Engineering, Department of Manufacturing Engineering and Management, Technical University of Denmark, DK-2800 Kgs. Lyngby, Denmark, and Risø National Laboratory, DK-4000 Roskilde, Denmark

Received March 4, 2003; Revised Manuscript Received May 5, 2003

ABSTRACT: Transient and steady elongational viscosity has been measured for two narrow molar mass distribution polystyrene melts of molar masses 200 000 and 390 000 by means of a filament stretching rheometer. Total Hencky strains of about five have been obtained. The transient elongational viscosity rises above the linear viscoelastic prediction at intermediate strains, indicating strain hardening. The steady elongational viscosities are monotone decreasing functions of elongation rate. At elongation rates larger than the inverse reptation time, the steady elongational viscosity scales linearly with molar mass at fixed elongation rate.

1. Introduction

The linear viscoelastic (LVE) properties of narrow molar mass distribution (MMD) linear polymers have been thoroughly investigated both experimentally and theoretically. Important insight was obtained from investigations of the scaling of zero shear rate viscosity, η_0, with molar mass, M. For a wide range of predominantly linear polymers it was shown[1] that $\eta_0 \sim M$ for $M < M_e$ and $\eta_0 \sim M^{3.4}$ for $M > M_e$, where M_e is the entanglement molar mass. Onogi et al.[2] reported LVE measurements of a series of anionically synthesized polystyrenes ranging from below M_e to well above M_e, showing a more or less well-defined platau modulus independent of molar mass for $M > M_e$.

The dependence of the zero shear rate viscosity on molar mass below M_e can be explained in terms of the Rouse model[3] or the Kramers model.[4] The key development for the understanding of the molar mass scaling above M_e was the Doi−Edwards (DE) model.[5] On the basis of the reptation idea,[6] the basic DE model predicts a molar mass dependence to the power of 3. The concept of contour length fluctuations[7] can be used[8] to explain a gradual transition from $\eta_0 \sim M^{3.4}$ just above M_e to $\eta_0 \sim M^3$ for $M \gg M_e$. The concept of double reptation[9,10] has proven powerful for the development of mixing rules.

The situation is less satisfactory for the nonlinear properties. In elongational flow, the DE model with the so-called independent alignment approximation for linear polymers predicts an upper limit to the tensile stress equal to 5 times the elastic modulus in small deformations, G_N. This limiting stress is a consequence of the assumption of instantaneous chain retraction whereby the stress becomes associated with orientation alone. To remedy this and other limitations of the model, Marrucci and Grizzuti[11] introduced the idea of chain stretching which has been incorporated in several reptation-based models.[12−15] However, none of these models have yet been compared with measurements of strong elongational flow of marrow MMD polymer melts. Indeed, the major limitation to progress in the understanding of the nonlinear properties in elongational flow seems to be the scarcity of data for well-characterized narrow MMD linear polymer melts.

Measurements of polymer chain conformation during elongational flow have been performed by small-angle neutron scattering.[16,17] The measurements performed on narrow MMD polystyrenes show that the macroscopically measured stress can be related to a network model with a strain tensor determined from the scattering experiments. The investigations were, however, limited to a maximum stretch ratio of about 3 and low elongation rates.

Polystyrene melts have been investigated also by rheooptical methods.[18,19] In particular, Venerus et al.[19] investigated a polydisperse polystyrene of weight-average molar mass $M_w = 335\,000$ and polydispersity $M_w/M_n = 2.85$. Up to a total tensile stress of about 1 MPa their measurements are in agreement with the stress optic rule, which for this flow dictates linearity between tensile stress and birefringence. For stresses larger than about 1 MPa they found significant deviations from the stress-optic rule in the form of a gradual saturation of the birefringence. They interpreted this to mean that the polymer chains were approaching full extension at the highest stresses obtained. On the basis of a simple model for chain stretching, they were able to formulate a criterion for the failure of the stress-optic rule. For narrow MMD linear polymers it is predicted that full chain extension is approached when the stress is of order $N_K G_N$, where N_K is the number of Kuhn steps between entanglements.

Measurements of a range of polystyrene melts[20,21] have demonstrated that the nonlinear elongational viscosity is quite sensitive to polydispersity. In fact, the presence of even small amounts of a high molar mass fraction may show up in the form of strain hardening of the melt.[20] In this work we have synthesized two narrow MMD polystyrene samples in which we have specifically taken care to avoid the formation of a high molar mass fraction. We present mesurements of transient elongational viscosity up to total Hencky strains of about 5. Hencky strain is defined as $\epsilon = \ln(\lambda)$ where $\lambda = L/L_0$ is the stretch ratio, L_0 being the initial length and L the final length. Our experimental method differs from previous methods for polymer melts in that we use a filament stretching rheometer[22] (FSR) designed to operate at elevated temperatures. The FSR has the

[†] Department of Chemical Engineering, Technical University of Denmark.
[‡] Department of Manufacturing Engineering and Management, Technical University of Denmark.
[§] Risø National Laboratory.

10.1021/ma034279q CCC: $25.00
Published on Web 06/20/2003

advantage compared to conventional techniques for elongational rheometry that the location of the necking can be predicted. This critical region can then be monitored and the plate motion adjusted online in such a way as to obtain a constant stretch rate at the neck. The stress in the region is subsequently deduced from a force balance.

2. Experimental Section

2.1. Synthesis and Chromatography. The two polystyrene samples PS200K and PS390K were prepared by anionic polymerization.[22] The molar mass was determined by size exclusion chromatography (SEC) with toluene as the eluent and employing a column set consisting of a 5 μm guard column and two 300 × 8 mm^2 columns (PLgel Mixed C and Mixed D). The system is equipped with a triple detector system (a combined Viscotek model 200 differential diffractive index (DRI) and differential viscosity detector plus a Viscotek model LD 600 right angle laser light scattering detector (RALLS)). On the basis of calibration with narrow polystyrene standards, the values of M_w and M_w/M_n were determined to be 200 kg/mol and 1.04 for PS200K and 390 kg/mol and 1.06 for PS390K. Molar masses based on direct use of the DRI and RALLS signals were within error identical to the values obtained by calibration. The presence in the SEC setup of the RALLS detector enhances sensitivity toward high molar mass impurities. No such impurities were detectable.

2.2. Mechanical Spectroscopy. We performed small-amplitude oscillatory shear to obtain an accurate determination of the linear viscoelastic properties of the polystyrene melts. We used a plate−plate geometry on an AR2000 rheometer from TA Instruments. The measurements were performed at 130 and 150 °C for both melts and at 170 °C for the high molar mass polystyrene melt. Using these data, we fitted the temperature shift factor a_T to the WLF equation

$$\log a_T = \frac{-c_1^0(T - T_0)}{c_2^0 + (T - T_0)} \tag{1}$$

where $c_1^0 = 8.86$, $c_2^0 = 101.6$K, $T_0 = 136.5$ °C, and T is temperature in °C. All data were shifted to a single master curve at 130 °C using the time−temperature superposition procedure.[4]

2.3. Extensional Viscosity Measurements. Extensional viscosity was measured using a filament stretching rheometer capable of measuring at high temperatures.[24] The polymers were dried and subsequently molded into cylindrical-shaped samples with radius $R_0 = 4.5$ mm and height $L_0 = 2.5$ mm. The molding process was performed in two steps. To get rid of the excess air, the powder was pressed into plates at room temperature. These plates were placed on top of a $R_0 = 2.5$ mm thick stainless steel plate with holes of radius $R = 4.5$ mm in it. The polymers were then pressed into the holes by a Carver hydraulic press. The PS200K was pressed at 150 °C and the PS390K at 170 °C. The temperatures were chosen as low as possible to prevent degradation and still high enough to have reasonable relaxation time. The duration of the molding process was about 2 min, and the polymers were checked for degradation after the molding by SEC. Samples for oscillatory shear measurements were produced in a similar way.

During an experiment, the radius $R(t)$ and axial force $F(t)$ in the filament were measured as a function of time. From the measurement of radius, the average strain rate could be estimated by fitting an exponential function $R(t) = R_0 \exp(-\dot{\epsilon}_0 t/2)$. The deviation between measurements and fit was never above ±4% and was usually within ±1%. When the average strain rate had been established, the transient elongational viscosity $\bar{\eta}^+(t)$ was calculated using

$$\bar{\eta}^+(t) = \frac{F(t)}{\pi R(t)^2 \dot{\epsilon}_0} \tag{2}$$

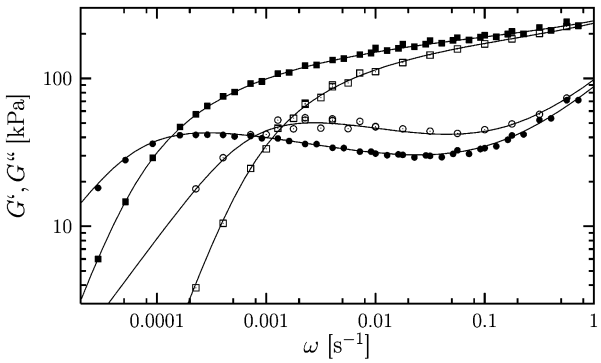

Figure 1. Linear viscoelastic data. The measurements on the polystyrene melts were performed at 130, 150, and 170 °C. The data are all time−temperature shifted to 130 °C. Squares are the loss modulus (G'') and circles are the storage modulus (G'), both as a function of the angular frequency, ω. Open and closed symbols are data for the polystyrene melt with M_w = 200 000 g/mol and M_w = 390 000 g/mol, respectively.

The major problem in performing the experiments was the inability of the samples to adhere to the end-plates of the rheometer. We found, however, that by coating the end-plates with some of the sample polymer, good adhesion could be achieved. To coat the end-plates, a droplet of a solution of polystyrene in tetrahydrofuran (THF) was placed on the end-plates. After evaporation of the THF, a thin layer of the polystyrene was left on the surface of the plate. The sample was then placed on top of the bottom plate and heated to 170 °C, and the upper plate was pressed on top of the sample. After relaxation of the initial pressure, the coating and sample polymer had sufficient time to diffuse into each other, and good adhesion was achieved. To increase the maximum obtainable stress in the middle of the filament even more, the end-plates were moved slowly apart until the center radius was about half of the initial radius. This dogbone shape was alowed to relax before the stretching experiment started. As the total force in the filament scales as the center radius squared, higher stresses can then be achieved in the middle of the filament for a given force of adhesion at the end-plates. This technique does rely on the high viscosity of the polystyrene melt which gives a time scale for sagging, $\eta_0/L_0\rho g$ (where ρ is density and g gravitational acceleration), much longer than the duration of the experiment. The use of the prestretch avoids an initial reverse squeeze flow. As a result, the transient measurements may be used uncorrected from zero strain.

The measurements were performed at temperatures 130 and 150 °C for both samples in order to examine the effects of dissipative heating. These temperatures were chosen such that the characteristic times of interest would lie in the strain rate range of the instrument.

3. Material Functions

3.1. Linear Viscoelasticity. In Figure 1 the loss modulus, G'', and storage modulus, G', of the two polystyrene melts are shown as a function of the angular frequency ω at a temperature of 130 °C. To describe the data, we use the continuous spectrum of Baumgaertel, Schausberger, and Winter.[25] The relaxation modulus, $G(s)$, is derived from the spectrum $H(\lambda)$ as follows:

$$G(t) = \int_0^\infty \frac{H(\lambda)}{\lambda} \exp(-t/\lambda)\, \mathrm{d}\lambda \tag{3}$$

$$H(\lambda) = [\, H_1\lambda^{n_1} + H_2\lambda^{-n_2}]h(1 - \lambda/\lambda_0) \tag{4}$$

where $h(\cdot)$ is the Heaviside step function. The term with H_1 describes the rubbery behavior at low and interme-

Table 1. Melt Properties at 130 °C

M_w	200 000 g/mol	390 000 g/mol
M_w/M_n	1.04	1.06
λ_0	1900 s	21000 s
n_1	0.22	0.16
n_2	0.7	0.7
$H_1\lambda_0^{n_1}$	53 200 Pa	41 700 Pa
$H_2\lambda_0^{-n_2}$	119 Pa	20 Pa
$G_N = H_1\lambda_0^{n_1}/n_1$	242 kPa	257 kPa
η_0	84 MPa s	755 MPa s
$\lambda_a \approx \lambda_0(1+n_1)/(2+n_1)$	1040 s	11 300 s

diate frequencies, while the term with H_2 describes the glassy behavior at the largest frequencies. We use the same cutoff value λ_0 for the distribution of relaxation times for both parts of the spectrum for simplicity. In the absence of glassy modes, the parameter n_1 is the absolute value of the slope of log G'' as a function of log ω in intermediate region where G'' decreases as a function of frequency. The parameter n_2 is the slope of log G'' as a function of log ω for $\omega \to \infty$. The parameters in the spectrum determined from the linear viscoelastic properties of the melt using a least-squares method[27] are given in Table 1. In addition in Table 1, we give three quantities derived from the spectrum as follows:

The plateau modulus, G_N, is computed as follows:

$$G_N = \frac{H_1\lambda_0^{n_1}}{n_1} \tag{5}$$

The plateau modulus is obtained as $G(0)$ where the glassy part of the spectrum has been excluded. The motivation for the use of $G(0)$ becomes clear when the expression for the stress tensor is formulated as a memory integral of the history of a strain tensor multiplied by the memory function. The plateau modulus defined above is then the elastic modulus in fast deformation of the hypothetical material in which the glassy behavior is neglected.

Our expression is in agreement with the integral involving the loss modulus given by Ferry,[26] the two expressions being related by a Fourier transformation. However, in practice, the methods differ in the way the glassy behavior is filtered out. The introduction of data directly in the Fourier integral[26] requires the additional choice of an upper limit of the integral, while our prefiltering of the modulus into a rubbery and a glassy contribution enables the extension of the Fourier integral to infinity by excluding the glassy part.

The plateau moduli estimated for the two molar masses differ by about 5%, which is well within experimental accuracy. Note that both values are somewhat higher than one might have extracted from a visual observation of the $G'(\omega)$ curve in Figure 1. We use an average value of $G_N = 250$ kPa in the following. With this value we compute a molecular weight between entanglements, M_e, defined[26] by analogy with rubber elasticity: $G_N = \rho RT/M_e$. This gives $M_e = 13\,300$ g/mol resulting in $Z = 15$ entanglements for PS200K and $Z = 29$ for PS390K. The relation between G_N and M_e by Ferry[26] is not the only one possible choice. The DE model without the independent alignment assumption[5] (IAA) gives the relation $G_N = {}^4/_5\rho RT/M_e$ while the DE model with the IAA invoked gives[3] $G_N = {}^3/_5\rho RT/M_e$. Fetters et al.[28] use the former of these two relations. However, they use $G_N = 200$ kPa for polystyrene, whereby they in fact obtain the same value of $M_e = 13\,300$ g/mol used here.

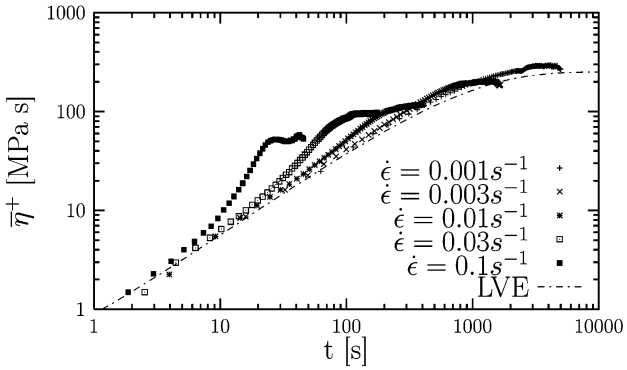

Figure 2. Transient extensional viscosity of PS200K measured at strain rates $\dot\epsilon = 0.1$, 0.03, 0.01, 0.003, and 0.001 s^{-1} starting from the left. Measurements were performed at 130 °C.

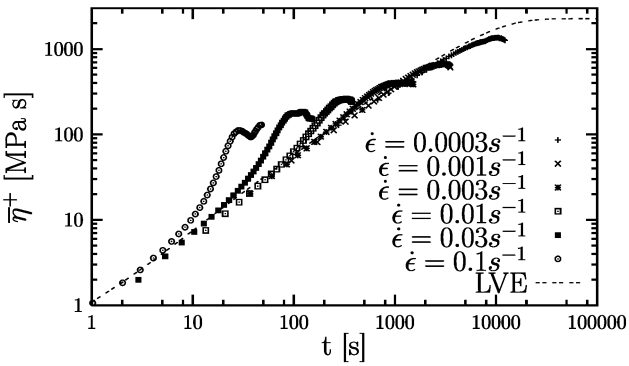

Figure 3. Transient extensional viscosity of PS390K measured at strain rates $\dot\epsilon = 0.1$, 0.03, 0.01, 0.003, 0.001, and 0.0003 s^{-1} starting from the left. Measurements were performed at 130 °C.

The zero shear rate viscosity is computed as follows:

$$\eta_0 = \int_0^\infty G(s)\,ds = H_1\lambda_1^{n_1+1}/(n_1+1) + H_2\lambda_2^{1-n_2}/(1-n_2) \tag{6}$$

We also note that the zero shear rate viscosities scale with molar mass to the power 3.3 relative to one another, which again is within experimental accuracy of the expected behavior.

The characteristic time for the melts is computed as follows:[4]

$$\lambda_a = \frac{\int_0^\infty G(s)s\,ds}{\int_0^\infty G(s)\,ds} \approx \lambda_0(1+n_1)/(2+n_1) \tag{7}$$

In this definition we include only the rubbery part of the spectrum. For later use we note that with the definition above the characteristic time for the DE model would become $\lambda_a = \pi^2\tau_d/10$, where τ_d is the reptation time. Since $\pi^2/10 \approx 1$, the characteristic time defined above is equal to the reptation time of the basic DE model for practical purposes.

3.2. Start-Up of Elongational Flow. In Figures 2 and 3 we plot the measured transient elongational viscosity $\bar\eta^+(t)$ for the PS200K and PS390K along with predictions from LVE. All elongational viscosity measurements were performed at 130 °C while the LVE predictions were based on the parameters in Table 1. In both plots there is agreement between measurements and LVE predictions up to a certain magnitude of strain.

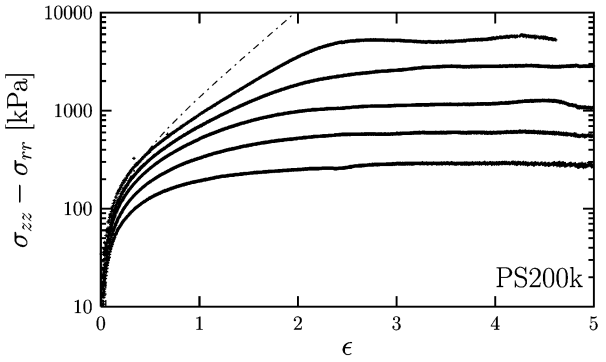

Figure 4. Same data as in Figure 2 plotted as stress vs Hencky strain. Upper curve is the highest strain rate. The thin line is the neo-Hookean elastic stress prediction with plateau modulus shown in eq 8.

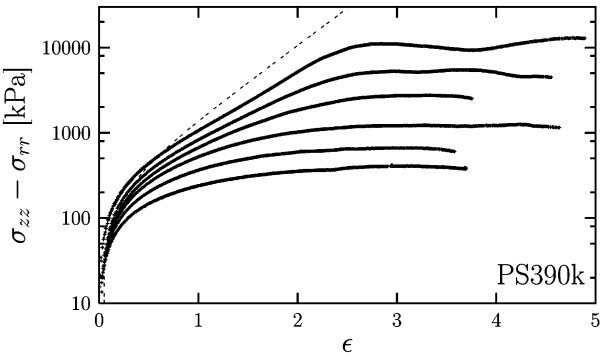

Figure 5. Same data as in Figure 3 plotted as stress vs Hencky strain. Thin line as in Figure 4.

The elongational viscosity reaches a steady state in all series. The plateau values of stress are constant within ±5% for about 1−2 strain units, except the series at $\dot{\epsilon} = 0.1\ s^{-1}$ in Figure 3, where the deviation is ±10%. Fluctuations in the steady-state values are correlated with changes in the instantaneous strain rate. It is seen that while all steady-state values are below $3\eta_0$ the transient elongational viscosity rises above LVE at intermediate strains.

As an alternative representation, we plot the same data as stress vs strain in Figures 4 and 5. In this representation the duration of the steady-state elongational viscosity is more apparent. Indeed, it is seen that all plateau values are kept for 1−2 Hencky strain units. The measurements for PS200K extend to a Hencky strain of 5 whereas the measurements for PS390K stop earlier. The reason for this difference is not related to the polymers but is due to an improvement in the control scheme of the end-plate movement.

4. Discussion

4.1. Implications of Stress Levels. In addition to the stress measurements in Figures 4 and 5, we have drawn the neo-Hookean stress prediction based on the plateau modulus:

$$(\sigma_{zz} - \sigma_{rr}) = G_N(\lambda^2 - \lambda^{-1}) \tag{8}$$

Here σ_{zz} and σ_{rr} are the axial and radial stress components, respectively. This stress difference would correspond to an equivalent affinely deforming network without relaxation. We have not observed any stresses above this prediction, which we take as a sign that the stretch rates are below those at which glassy modes would be excited.

The maximum stresses in Figures 4 and 5 are about $40G_N$. This is well above the value of $5G_N = 1.25$ MPa, which is the maximum stress obtained by orientation according to the basic DE model. As we have just concluded that the stress is not of glassy origin, we take this as a signature of substantial chain stretching in the polymers.

We may also compare the stress levels with the prediction for near full chain extension and failure of the stress-optic rule suggested by Venerus et al.[19] With the number of Kuhn steps between entanglements $N_K = 22$ for polystyrene[12] the critical stress would be 5.5 MPa, which is reached for both melts and exceeded for PS390K. We take this as a measure, albeit an indirect one, that the chains have reached near full extension.

Finally, we note that for the experiments with the highest stretch rates there seems to be a reasonably well-defined strain that marks the transition from transient behavior to a steady state. If we assume that the deformation in the transient process is affine, we can derive an estimate of the Hencky strain at which the chains on average become fully extended. We model the polymer as a Kramers chain composed of N freely jointed Kuhn steps; the ratio of the fully extended chain to the root-mean-square end-to-end distance becomes $\sqrt{N}$. Hence, on average the maximum Hencky strain of an affine deformation would be $\epsilon_m = \ln \sqrt{N} = \ln \sqrt{N_K Z}$. Here, N_K is the number of Kuhn steps between entanglements and Z is the number of entanglements. In the latter expression, ϵ_m is expressed as alternatively the sum of two terms: the strain needed to orient all segments end to end ($\ln \sqrt{Z}$) and the strain needed to stretch all segments ($\ln \sqrt{N_K}$). With $N_K = 22$ for polystyrene the estimates for ϵ_m become 2.9 and 3.2 for PS200 and PS390, respectively. These values are both somewhat higher than the observed values of transition to steady state, while the difference (0.3 Hencky strain units) seems to correspond reasonably well with the behavior of the two melts.

4.2. Low Deborah Number Scaling. We turn now to a consideration of the steady elongational viscosity $\bar{\eta}(\dot{\epsilon})$ as a function of elongation rate. We present the data in nondimensional form as Trouton ratio ($Tr = \bar{\eta}/\eta_0$) as a function of Deborah number ($De = \lambda_a \dot{\epsilon}$) defined with the characteristic time from the LVE spectrum. Keep in mind that both η_0 and λ_a have been found to scale approximately as molar mass to the power 3.4, as expected in the small Deborah number limit.

We note from Figure 6 that the data for PS200K do correctly reach a limiting Trouton ratio of 3 for small De, while for PS390K it has not been possible to reach this limit. In addition, we see that the departure from a Trouton ratio of 3 seems to occur at about De = 3 for both melts. This indicates that the departure from low Deborah number behavior is correctly described by λ_a, which scales as $M^{3.4}$. However, for De > 1 the data no longer overlap, indicating the onset of a process that does not scale as $M^{3.4}$.

For comparison, we have included the prediction of the DE model. In this plot we have used the reptation time $\tau_d = 10\lambda_a/\pi^2$. The asymptotic relation for $\bar{\eta}$ becomes $5G_0/\dot{\epsilon}$. Since $\eta_0 = (\pi^2/12)G_0\tau_d$ in the DE model,[3] the asymptotic relation for the Trouton ratio becomes $6/De$ in the present notation. We have already seen in section 4.1 that the stresses become higher than the maximum

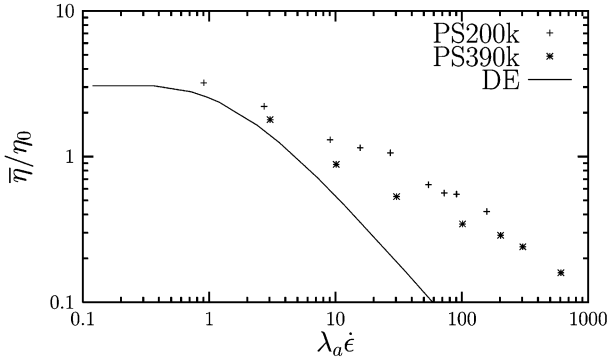

Figure 6. Steady-state extensional viscosity normalized with zero shear viscosity as a function of Deborah number. All measurements were performed at 130 °C.

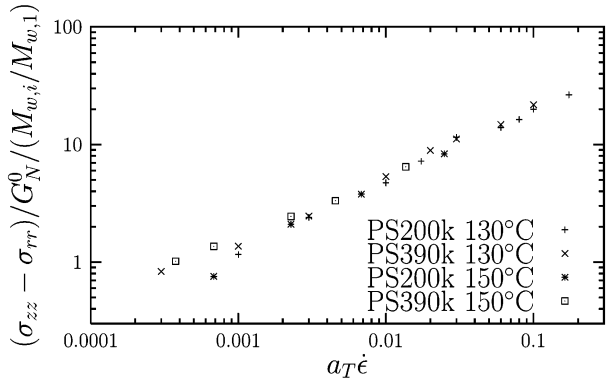

Figure 7. Steady-state stresses as a function of elongation rate for polystyrene $M_w = 200\,000$ ($i = 1$) and $M_w = 390\,000$ ($i = 2$) measured at $T = 130$ °C and $T = 150$ °C. The elongation rates have been shifted to $T = 130$ °C with the shift factor a_T. The stresses have been shifted to $M_w = 200\,000$ with a linear scaling in molecular weight.

stress in the DE model; it is not surprising that the DE model does not resolve the data. We would like to point out, however, that the DE model seems to underpredict stress for all elongation rates larger than the inverse reptation time.

Measurements of elongational viscosity of polydisperse polymer melts[20] and polymer solutions[29] show Trouton ratios above 3 and a nonmonotone viscosity function. This is in qualitative difference to our measurements for narrow MMD melts. It would be interesting, therefore, to study mixing rules in both the linear and nonlinear regime.

4.3. High Deborah Number Scalings. As an alternative to the representation in Figure 6, we have plotted the steady flow data as a function of elongation rate $\dot{\epsilon}$ in physical units. In so doing, it is possible to make the data overlap if the viscosities (or stresses) are scaled linearly with molar mass. This is illustrated in Figure 7, where we plot the stress for PS200K together with the stress for PS390K multiplied by 200/390. Furthermore, we also include stresses measured at 150 °C but shifted to 130 °C with the shift factors from eq 1. It is seen that practically all data collapse on a single curve.

The collapse of the data may be interpreted to mean that the time constant in the underlying dynamics process is independent of chain length. The observation that the stresses scale linearly in molar mass may suggest that the steady state is not controlled by reptation. We have already mentioned that the zero shear rate viscosity scales linearly in molar mass in the absence of entanglements. However, it seems unlikely that arguments for zero shear rate viscosity would be relevant for this highly nonlinear situation. Conversely, if one assumes that all molecules are oriented along the axis and stretched nearly to full extension, the implication of the linear scaling of stress in molar mass is that the tension in the molecules scales linearly with molar mass. To show this use the stress expression $\sigma_{zz} = n\langle R_z F_z\rangle$, where n is the number density of polymers, R_z is the end-to-end distance of the highly oriented and almost fully stretched molecule, and F_z is the connector force transmitted in the molecules. The brackets indicate average values, which however may be disregarded if all molecules are indeed highly oriented and stretched as assumed. Now since we have narrow MMD polymers, $n \sim M^{-1}$ and $R_z \sim M$ near full extension. The observed linear scaling of σ_{zz} at fixed $\dot{\epsilon}$ would therefore imply a linear scaling of F_z. However, this interpretation of the data hinges on the assumption of near full extension. To test that assumption, more direct measurements of molecular orientation and stretching would be needed.

For elongation rates above the inverse reptation time, the stress increases approximately as $\dot{\epsilon}^{0.5}$. Therefore, the representation in Figure 7 may be expressed in the form

$$\frac{\sigma_{zz} - \sigma_{rr}}{Z} \sim \sqrt{\dot{\epsilon}} \tag{9}$$

This relation may be formulated alternatively as $\sigma_{zz} - \sigma_{rr} \sim \sqrt{\dot{\epsilon} Z^2}$. Hence, in place of scaling the stress as in Figure 7, we could have scaled the elongation rates with the square of the molecular weight. Since the characteristic time for the Rouse model, τ_R, increases with the square of the molecular weight, such a representation is equivalent to using an elongation rate made nondimensional with τ_R. However, in such a plot we see no sign of changes in qualitative behavior when the nondimensional elongation rate is of order unity.

4.4. Thermal Effects. During the stretching of a polymer sample, a considerable amount of work is applied to the sample which at adiabatic conditions would result in a considerable temperature increase. However, it is implicit in the reporting of material functions that these apply to isothermal conditions. Therefore, it is important to suppress a temperature increase by radiative and convective heat transport. The convective heat transport is imposed by a circular array of 44 N_2 jets that impose a gas flow past the filament.

The key parameter needed to estimate thermal effects is the heat-transfer coefficient from the filament to the surroundings. Since the emissivity of polymers is close to unity in the infrared range, the radiative heat transfer coefficient can be estimated as $h_r = 4\sigma_r T_0^3 = 15$ W/(m^2 K). Although this does represent a absolute lower limit for the heat transport, radiation alone is not sufficient to keep the filament isothermal. The convective heat transfer coefficient is more difficult to compute, since it depends on the turbulent flow around the filament generated by the nitrogen jets. We estimate that the total heat transfer coefficient, h_w, including convection could be of the order of magnitude 100 W/(m^2 K).

To estimate radial temperature gradients in the filament, we introduce the Biot number $Bi = h_w R/k_{PS}$, where k is the thermal conductivity of polystyrene and R is the radius of the filament. With $k_{PS} = 0.17$ W/(m K) and $R = 1.5$ mm, we find $Bi \approx 0.9$. Thus, during start-up, there will exist a temperature gradient inside the

fluid. As the experiment proceeds, the radius of the filament decreases and internal temperature gradients in the filament will become negligible. To get a simple estimate of the thermal effects, we therefore assume that the filament has a uniform temperature T.

A simple balance for the temperature T in the filament may be formulated as follows:

$$\rho C_p \frac{\mathrm{d}T}{\mathrm{d}t} = \dot{\epsilon}[\sigma_{zz}(t) - \sigma_{rr}(t)] - \frac{2h_w(T - T_b)}{R} \quad (10)$$

Here ρ and C_p are the density and heat capacity of the melt; h_w is the heat transfer coefficient between the filament the surroundings assumed to have uniform temperature T_b. The first term on the right side is the generation term while the second term is the loss term. On the basis of this equation, we have estimated the maximum temperature rise to be about 2 °C so the maximum deviation in the strain rate is less than 50% for the highest strain rates and much less at lower strain rates.

To get another appreciation of the effects, we rewrite the balance with Hencky strain as independent variable:

$$\rho C_p \frac{\mathrm{d}T}{\mathrm{d}\epsilon} = [\sigma_{zz}(\epsilon) - \sigma_{rr}(\epsilon)] - \frac{2h_w(T - T_b)}{\dot{\epsilon} a_T R_0} a_T \exp(\epsilon/2) \quad (11)$$

In this form it is also explicit that the loss term increases as the Hencky strain increases. We now compare two experiments performed at 130 and 150 °C but with the same value of $\dot{\epsilon}a_T$. The generation term involving the stress difference is more or less the same for the two experiments. On the other hand, the loss term is a factor $a_T(130)/a_T(150) \approx 40$ bigger for the experiment at 130 °C. We therefore interpret the agreement between experiments performed at 130 and 150 °C up to $\dot{\epsilon}a_T \approx 0.02\ \mathrm{s}^{-1}$ as an indication that thermal effects are negligible below this value. Moreover, since the generation term increases as $\sqrt{\dot{\epsilon}}$, we continue the measurements at 130 °C a factor of $\sqrt{40} \approx 6$ higher in $\dot{\epsilon}a_T$ than the measurements at 150 °C.

5. Conclusions

We have used a filament stretching apparatus to measure transient and steady elongational viscosity of narrow MMD polystyrene melts of molar mass 200 000 and 390 000.

Transient elongational viscosities agree with predictions from linear viscoelasticity within the linear region. At intermediate strains the transient viscosity rises above the LVE prediction, while the steady-state elongational viscosity is below $3\eta_0$.

The steady elongational viscosity is a monotone decreasing function of the elongation rate, $\dot{\epsilon}$. The transition from $3\eta_0$ to nonlinear behavior occurs at an elongation rate that is well predicted by the inverse of the time constant λ_a, which for practical purposes is equal to the reptation time of the DE model. At elongation rates larger than λ_a^{-1} the steady elongational viscosity scales linearly with molar mass at constant elongation rate. The steady elongational viscosity decreases approximately as $\dot{\epsilon}^{-1/2}$ for $\dot{\epsilon} > \lambda_a^{-1}$.

In closing, we would like to point out that the conclusions with regard to molar mass scaling are based on merely two samples. Thus, it would be highly desirable with a wider range of molar mass.

Acknowledgment. We thank senior scientist S. Ndoni and K. Szabo for performing the SEC tests. We also thank Professors H. C. Öttinger, R. G. Larson and T. C. B. McLeish for useful comments. The work was supported by a grant from the Danish Technical Research Council to the Danish Polymer Centre.

References and Notes

(1) Berry, G. C.; Fox, T. G. *Adv. Polym. Sci.* **1968**, *5*, 261−357.
(2) Onogi, S.; Masuda, T.; Kitagawa, K. *Macromolecules* **1970**, *3*, 109−116.
(3) Doi, M. *Introduction to Polymer Physics;* Clarendon Press: Oxford, 1992.
(4) Bird, R. B.; Armstrong, R. C.; Hassager, O. *Dynamics of Polymeric Liquids*; Wiley: New York, 1987; Vol. 1.
(5) Doi, M.; Edwards, S. F. *The Theory of Polymer Dynamics*; Clarendon Press: Oxford, 1986.
(6) de Gennes, P. G. *Scaling Concepts in Polymer Physics*; Cornell University Press: Ithaca, NY, 1979.
(7) Doi, M. *J. Polym. Sci., Polym. Phys.* **1983**, *21*, 667−684.
(8) Milner, S. T.; McLeish, T. C. B. *Phys. Rev. Lett.* **1998**, *81*, 725−728.
(9) Tsenglou, C. *ACS Polym. Prepr.* **1987**, *28*, 185−186.
(10) Des Cloizeaux, J. *Europhys. Lett.* **1988**, *5*, 437−442.
(11) Marrucci, G.; Grizzutti, N. *Gazz. Chim. Ital.* **1988**, *118*, 179−185.
(12) Fang, J.; Kröger, M.; Öttinger, H. C. *J. Rheol.* **2000**, *44*, 1293−1317.
(13) Mead, D. W.; Larson, R. G.; Doi, M. *Macromolecules* **1998**, *31*, 7895−7914.
(14) Schieber, J.; Neergaard, J.; Gupta, S. *J. Rheol.* **2003**, *47*, 213−233.
(15) Ianniruberto, G.; Marrucci, G. *J. Rheol.* **2001**, *45*, 1305−1318.
(16) Muller, R.; Picot, C.; Zang, Y. H.; Froelich, D. *Macromolecules* **1990**, *23*, 2577−2582.
(17) Muller, R.; Picot, C. *Makromol. Chem., Macromol. Symp.* **1992**, *56*, 107−115.
(18) Kotaka, T.; Kojima, A.; Okamoto, M. *Rheol. Acta* **1997**, *36*, 646−656.
(19) Venerus, D. C.; Zhu, S. H.; Öttinger, H. C. *J. Rheol.* **1999**, *43*, 795−813.
(20) Münstedt, H. *J. Rheol.* **1980**, *24*, 847−867.
(21) Takahashi, M.; Isaki, T.; Takigawa, T.; Masuda, T. *J. Rheol.* **1993**, *37*, 827−846.
(22) McKinley, G. H.; Sridhar, T. *Annu. Rev. Fluid Mech.* **2002**, *34*, 375−415.
(23) Ndoni, S.; Papadakis, C. M.; Bates, F. S.; Almdal, K. *Rev. Sci. Instrum.* **1995**, *66*, 1090−1095.
(24) Bach, A.; Rasmussen, H. K.; Hassager, O. *J. Rheol.* **2003**, *47*, 429−441.
(25) Baumgartel, M.; Schausberger, C.; Winter, H. H. *Rheol. Acta* **1990**, *29*, 400−408.
(26) Ferry, J. *Viscoelastic Properties of Polymers*; Wiley: New York, 1980; p 404, eq 5.
(27) Rasmussen, H. K.; Christensen, J. H.; Gottsche, S. *J. Non-Newtonian Fluid Mech.* **2000**, *93*, 245−263.
(28) Fetters, L. J.; Lohse, D. J.; Richter, D.; Witten, T. A.; Zirkel, A. *Macromolecules* **1994**, *27*, 4639−4647.
(29) Bhattacharjee, P. K.; Oberhauser, J. P.; McKinley, G. H.; Leal, L. G.; Sridhar, T. *Macromolecules* **2002**, *35*, 10131−10148.

MA034279Q